PREDICTION OF MATERIAL REMOVAL RATE IN DIE-SINKING ELECTRICAL DISCHARGE MACHINING

An Undergraduate Research Scholars Thesis

By

ALICIA GUTHRIE and STEPHANIE LEE

Submitted to the Undergraduate Research Scholars program at
Texas A&M University
in partial fulfillment of the requirements for the designation as an

UNDERGRADUATE RESEARCH SCHOLAR

Approved by Research Advisor: Dr. Wayne Hung

May 2017

Major: Manufacturing and Mechanical Engineering Technology

TABLE OF CONTENTS

Page

ABSTRACT

Prediction of Material Removal Rate in Die-Sinking Electrical Discharge Machining

Alicia Guthrie and Stephanie Lee
Department of Engineering Technology & Industrial Distribution
Texas A&M University

Research Advisor: Dr. Wayne Hung
Department of Engineering Technology & Industrial Distribution
Texas A&M University

This project proposes a new model for material removal rate (MRR) of conductive materials using die-sinking electrical discharge machining (EDM). Five different engineering materials were used in this study. Small holes were drilled by EDM and the hole dimensions were measured to determine the MRR on each material. The process parameters and material thermal properties were used to derive the empirical model. While the existing model predicts MRR with ~1000% error, the new model is much more accurate and can predict the MRR to ~ 70%.

ACKNOWLEDGEMENTS

We would like to thank Dr. Wayne Hung, Dr. Jorge Leon, Mr. Zhujian Feng, and Department of Engineering Technology and Industrial Distribution at Texas A&M University for support throughout this project.

NOMENCLATURE

EDM	Electrical Discharge Machining
HSLA	High Strength Low Alloy
MRR	Material Removal Rate
VMS	Vision Measuring System
A	Area under pulsed current and time curve
D	Thermal diffusivity
I_p	Peak current
K	Thermal conductivity
n	Total number of elements in an alloy
P	Proportional constant
Q	Electrical charge
Q_c	Electrical charge for each EDM pulsed current cycle
T_m	Melting temperature
T_{on}	On-time
T_{off}	Off-time
x_i	Volume percentage of the i^{th} element in an alloy

CHAPTER I

INTRODUCTION

In today's technology-saturated world, traditional and nontraditional machining techniques come together to make everything we have today possible. Electrical discharge machining (EDM) is a nontraditional method that uses electrical sparks between an electrode tool and a conductive workpiece to controllably remove minute amount of materials in successive sequences. The electrode can be a small wire that moves continuously through and cut the workpiece, or any desirable shape that "sinks" into a workpiece and form the negative shape of the electrode for dies and molds. Die-sinking EDM is used in this study.

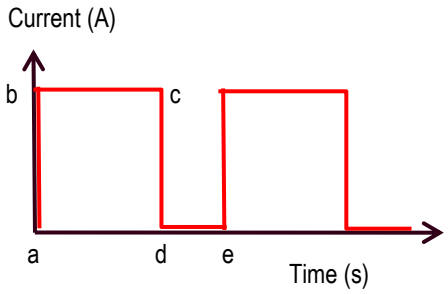

ab: peak current I_p
ad: on-time t_{on}
de: off-time t_{off}
ae: cycle T
ad/ae: duty cycle (duty factor)
1/ae: frequency

Figure 1: Pulsed current in EDM

A pulsed current is traditionally used in EDM. Figure 1 shows the theoretical pulsed current that flows across the electrodes. A bank of external capacitors is charged then electrically discharged during the on-time to generate simultaneous sparks that remove discrete amount of materials as debris. Such debris is then flushed away during the off-time to reveal a fresh workpiece surface for the next spark eroding cycle. Assuming a constant peak current, the area under the current-time plot is:

$$A = \int_0^T I(t)dt = \int_0^{t_{on}} I(t)dt = I_p t_{on} \quad (1)$$

This area *A*, therefore, is the cumulative charge *Q* that would be discharged to generate a spark. Most researchers consider peak current and on-time separately rather than combining them when studying the workpiece material removal rate (MRR).

The EDM process is slow since it removes minute amount of material in each spark between electrodes. It is desirable to have a mathematical model to predict the material removal rate (MRR) based on the material properties and process variables. The MRR for EDM was documented to be proportional to the peak current but not the shape of the current-time profile, i.e., the model is independent to both on-time and off-time (Weller, 1984):

$$MRR = \frac{664\, I_p}{{T_m}^{1.23}} \quad (2)$$

Where *MMR*: material removal rate (mm^3/s)

I_p: peak current (A)

T_m: workpiece melting temperature (°C)

In another study, Izwan et al. (2016), proposed the dependence of MRR on the electrical charge (product of peak current and on-time):

$$MRR = \frac{(I_p * T_{on})^{1.11}}{219\, T_m^{0.537}} = \frac{Q^{1.11}}{219\, T_m^{0.537}} \quad (3)$$

Where *MRR*: material removal rate (mm^3/s)

I_p: current (A)

T_{on}: on time (μs)

T_m: workpiece melting temperature (°C)

Q: charge (A μs)

Experimental data have shown the inaccurate prediction of MMR from equations (2 and 3); therefore, a new model is sought. The objective of this project is to derive a new model for MRR for EDM process while considering the workpiece material properties and all process variables.

CHAPTER II

METHODS

Material Preparation

Five different materials were selected with a wide range of melting temperatures since EDM is a thermal process. The chemical compositions of these materials are shown in Table 1.

Table 1: Chemical Compositions of Tested Materials
(Izwan et al, 2016; AZO; MakeItFrom; Rotometals)

Materials	*Weight %*
Aluminum 6061-T6:	96.7 Al, 0.6 Si, 1.0 Mg, 0.2 Cr, 0.15 Mn, 0.15 Ti, 0.27 Cu, 0.25 Zn, 0.7 Fe
HSLA Steel:	98.9 Fe, 0.80 Mn, 0.14 C, 0.1 Si 0.005 Ti, 0.004 V
Brass CA 360:	61.5 Cu, 0.35 Fe, 3.0 Pb, 35.5 Zn
R92 Pewter:	92 Sn, 8 Sb
ZA-8 Zinc aluminum:	89.8 Zn, 8.8 Al, 1.3 Cu, 0.075 Fe, 0.03 Mn, 0.006 Pb, 0.006 Cd, 0.003 Sn

Physical and mechanical properties of these materials are shown in Table 2. Thermal conductivity and diffusivity were found from difference sources or calculated from the following equation based on the principle of electrical conductivity:

$$\frac{100}{K_{alloy}} = \sum_{i=1}^{n} \frac{x_i}{K_i} \tag{4}$$

Where K_{alloy}: thermal conductivity of an alloy (W/m°K)

n: number of elements in alloy

K_i: thermal conductivity to the i^{th} element (W/m°K)

x_i: volume percentage of element i (%)

Table 2: Relevant Physical and Mechanical Properties
(Izwan et al, 2016; ASM; AZO; MakeItFrom; RotoMetals)

Properties	*6061-T6*	*HSLA*	*CA 360*	*R92*	*ZA-8*
Density (g/cm^3)	2.7	7.81	8.49	6.15	6.3
Hardness (Brinell)	95	138	60	--	85
Melting temp (°C)	582-652	1527	1050	241	375-404
Shear strength (MPa)	207	260	235	--	241
Yield strength (MPa)	276	380	310	--	206
Tensile strength (MPa)	300	450	400	30-50	221-255
Specific heat (J/g/°C)	0.876	0.446	0.38	--	0.435
*Thermal conductivity (W/m°K)	177	52	110	53^+	114.7
*Thermal diffusivity (mm^2/s)	73	14.9	34	38.3^+	418.5

*Estimated values from similar alloys (www.electronics-cooling.com)
$^+$Calculated values from equation (4)

Workpieces were obtained in as-rolled form, or cut from a cast ingot into plates of approximately 50 x 70 mm and thickness between 3-8 mm. Each sample surface was lightly sanded with 600-grit sand paper prior to each experiment to remove any possible contaminant that may interferes with the EDM process (Fig. 1).

Figure 2: Steel sample before and after sanding.

The Sodick K1C die-sinking EDM (Figure 2) was used to form holes with a rotating and hollow copper electrode (ø2 mm outside diameter and ø0.8 mm inside diameter). The constant electrode rotation speeds were measured four times by clocking the required times for 20 rotations to be 123, 119, 122, and 122 rpm. The peak current was set at 13A and 33A, while on-time was set at 20 μs and 28 μs, while the off-time was set at 4, 6, 10, 14, 20, and 28 μs. Other parameters were kept constants: 8 volt servo voltage regulator, 0.22 μF capacitor, Vitol-KS dielectric fluid (900 Ωcm resistivity, 0.925 m^2/s kinematic viscosity) for through electrode flushing. Machining times (15 s for thin plates and 18 s for thicker plates) were measured with a stop watch in previous study to produce a "blind" hole. In this study, the machining time was recorded when sparking was observed at the workpiece top surface at entrance hole and ended when sparking appeared at the exit end after drilling through the workpiece thickness. The clock started when the gap voltage experienced a significant drop as observed on an analog voltage gage. The sudden changes also coincided with the first sparking sound when the electrode approaching a workpiece. Each condition was repeated twice and two different operators performed the study independently using the same workpieces. All experiments were conducted in random sequence to minimize system error.

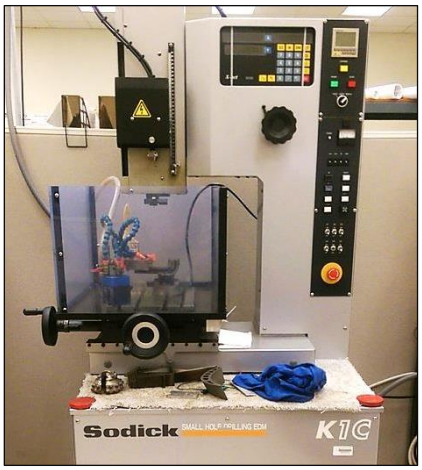

Figure 3: Sodik K1C Die-Sinking EDM Machine

Machining Procedure

The EDM system was first turned on and initialized. Before placing the sample in the clamp, the hollow electrode's length and quality was examined to make sure of steady flow of dielectric fluid. A workpiece was secured on a vise and mounted flush to the top of the vise. The system's conductivity was then confirmed by electrically connect the electrode and the workpiece. An audible beep and visual LED light would confirm the conductivity of the system. The electrode position was adjusted so that its tip was approximately 2-3 mm away from the workpiece and the machining cycle started. When completed, the electrode retracted above the workpiece and moved 2 mm away from previously drilled hole before starting the next hole. The EDM sparks in a typical experiment can be seen in Figure 3 below.

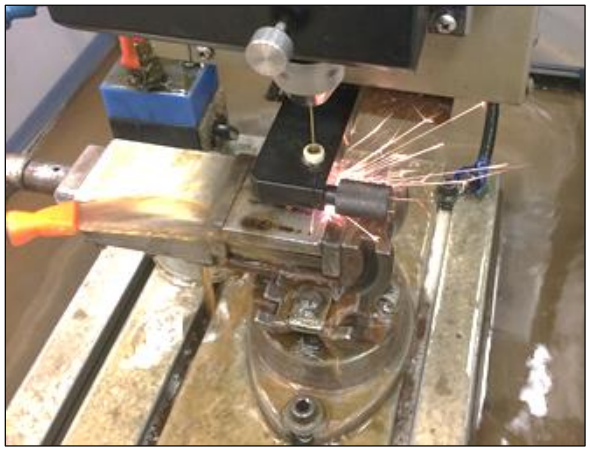

Figure 4: EDM'ing on a steel workpiece.

Post Machining Procedure

A workpiece was removed, wiped off remaining dielectric fluid, and cleaned ultrasonically in 70% isopropyl alcohol, and blown dry with compressed air. The hole dimensions were then measured for MRR calculation. Entrance and exit hole diameters were measured using the Mitutoyo Quick Scope Vision Measuring System (VMS). A hole was centered on the x-y axis and the contrast and focus were adjusted until there was uniform contrast around the hole. Then the "circle" function was selected. If the circle appeared uniform, the one-click circle tool was used. If the circle was not optimal, the manual-click tool was used by selecting at least three points on uniformly-contrast edges around the circle. Extrusions or possible corrosion or dirt were not included in the measurements. The measurements were repeated two or three times as necessary for each hole. The system and typical hole measurement are shown in Figures 5 and 6.

Figure 5: Mitutoyo Quick Scope Vision Measuring System

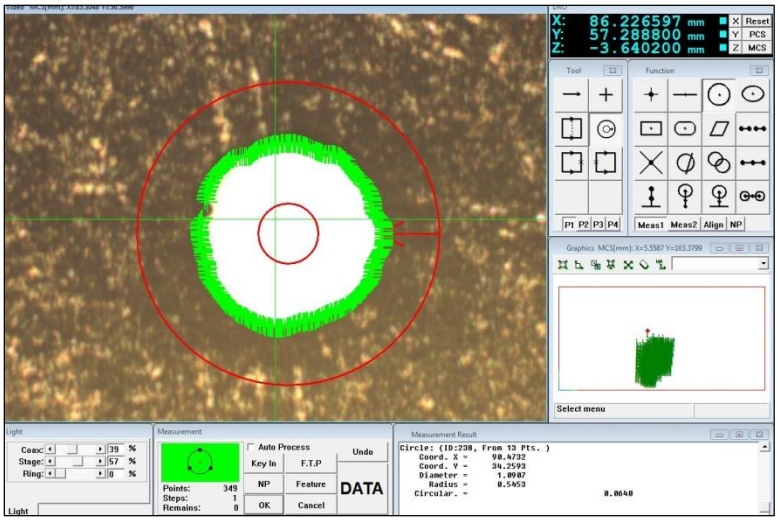

Figure 6: Typical hole diameter measurement

CHAPTER III

RESULTS AND DISCUSSION

Material Properties

Although data for materials can be found from published literature, thermal conductivity and thermal diffusivity are difficult to find for some engineering alloys. Rule of mixture gives satisfactory mechanical properties, but not thermal properties. Since thermal conductivity and diffusivity are analogous to electrical conductivity, so the first attempt was to calculate the thermal conductivity of an alloy based the using the known principles of electrical conductivity (equation 3). Appendix B details the calculations of three engineering alloys in this study:

- Thermal conductivity of ZA-8 zinc aluminum: calculated value of 118 vs published value of 114.7 W/m°K
- Thermal conductivity of CA360 brass: calculated value of 174.9 vs published value of 110 W/m°K.
- Thermal conductivity of Pewter R92: calculated value of 52.9 W/m°K. No published value was found for this alloy.

Experimental Material Removal Rate

Material removal rate is calculated as the ratio of the volume of removed material (based on diameters of entrance and exit holes and the plate thickness) and the machining time. The entrance diameter is slightly larger than that of the exit hole due to gradual wear of the cylindrical electrodes during the process. Figures 7-11 compare MRR results from two independent student operators. The "Group Number" corresponds to a set of specific EDM

process parameters; group numbers 1-6 correspond to low energy setting while 7-12 are for high energy setting (Appendix A). Referring to Figure 8, a wide spreading of data for steel is observed although both operators repeated their experiments twice. Data variation is worse when high current, therefore high energy spark, was used. Although each sample surface was hand sanded with 600-grit abrasive paper, it is suspected that sanding was inefficient to removal all corroded layer on the steel surface. Since corrosion process enhances quickly during EDM'ing, the non-conductive iron oxide would affect the drilling time and hole measurement results.

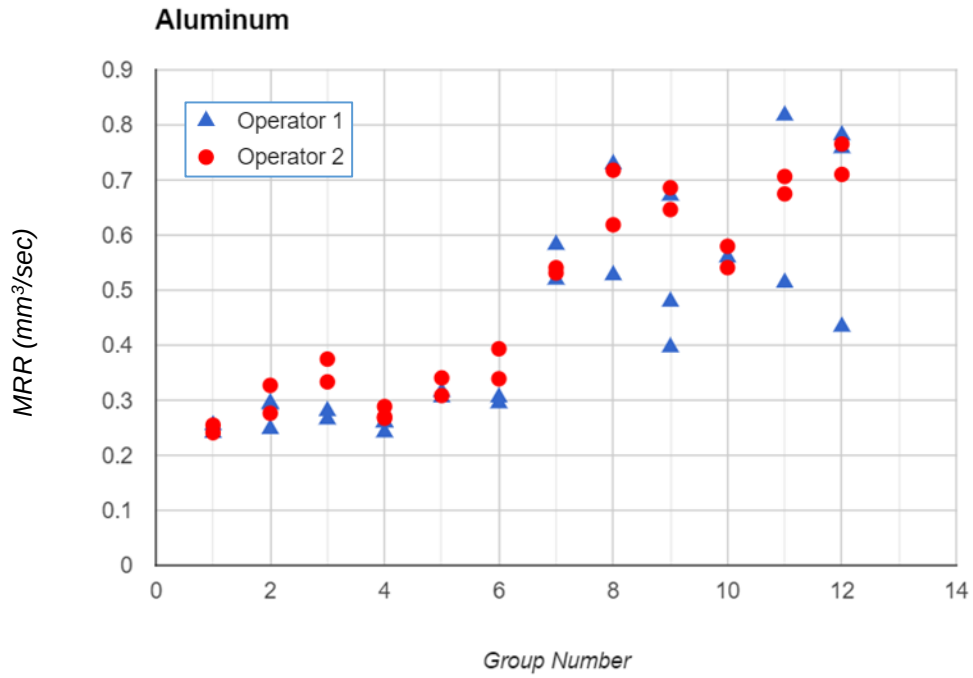

Figure 7: Material removal rate of 6061-T6 aluminum.

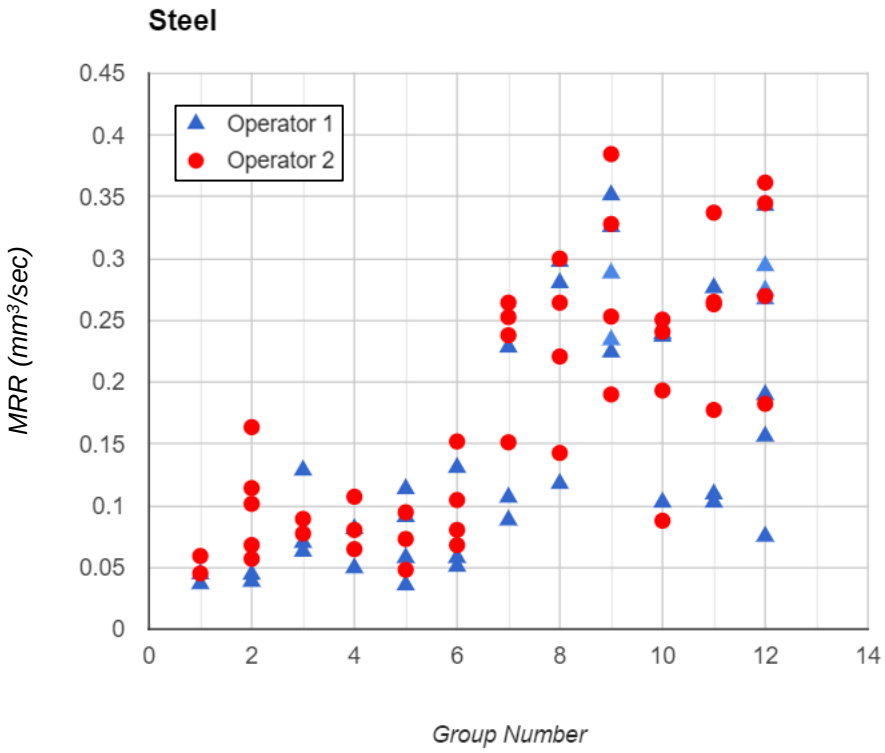

Figure 8: Material removal rate of HSLA steel.

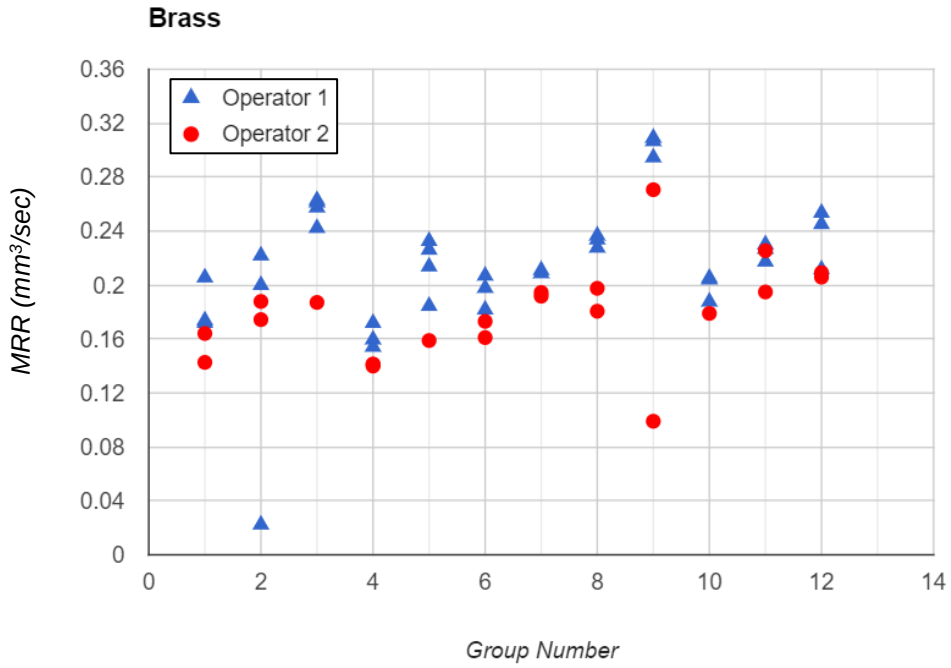

Figure 9: Material removal rate of CA 360 brass.

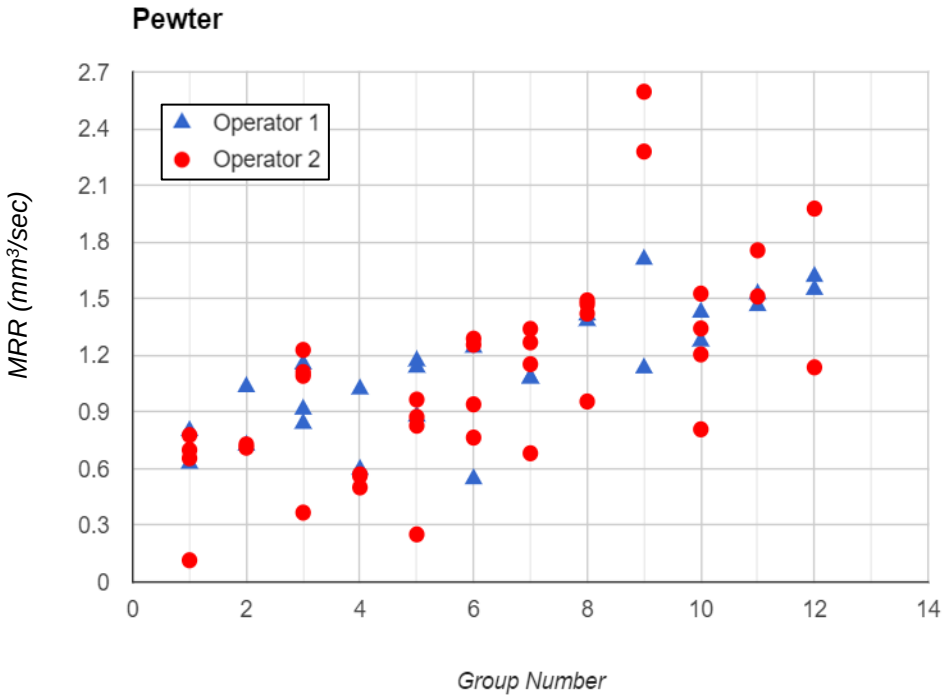

Figure 10: Material removal rate of R92 pewter.

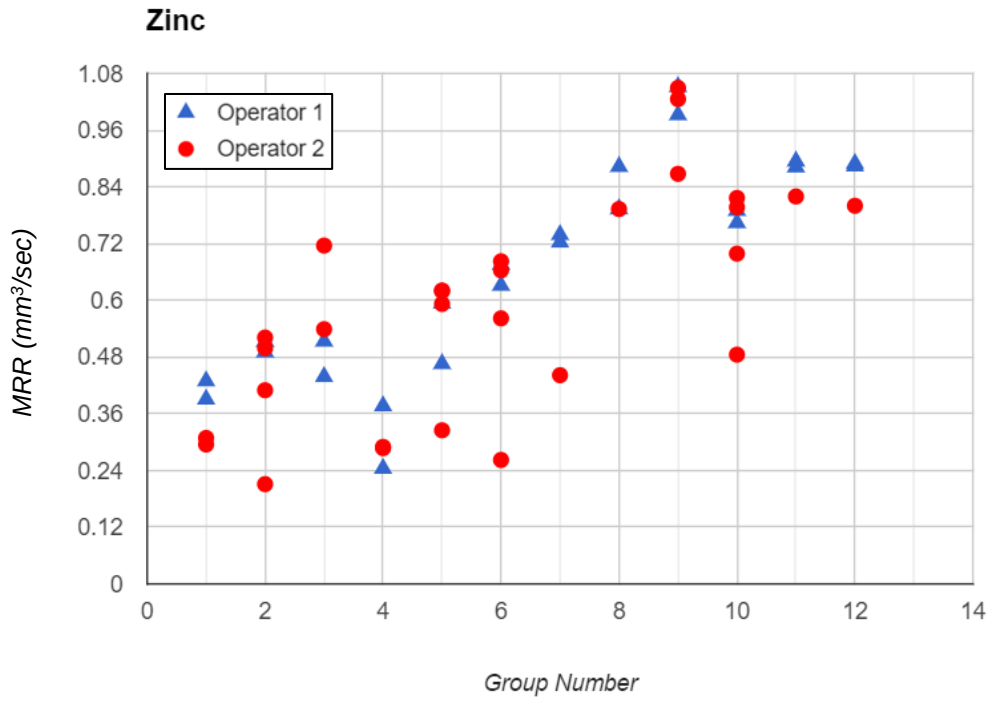

Figure 11: Material removal rate of ZA8 alloy.

MRR Model Derivation

Since EDM is an electrical and thermal process, equation (1) proposes the MRR depends on the current and workpiece melting temperature. This research extends this classical model and includes the charge per cycle --the effective charge and the duration at which a spark is energized – and is calculated from:

$$Q_c = I_p \, T_{on} \left(\frac{T_{on}}{T_{on} + T_{off}} \right) \tag{5}$$

Where Q_c: electrical charge per cycle

I_p: peak value of a square pulse current

T_{on}: on-time

T_{off}: off-time

Discussion

As expected, the workpiece thermal properties affect the MRR since successive EDM sparks heat and melt minute amount of workpiece material. Melting temperature, thermal conductivity and thermal diffusivity are included in the study. A sample was hand sanded before an experiment, ultrasonically cleaned in alcohol to remove corroded products inside a hole after EDM'ed, and then measured hole dimension to minimize error. However, EDM results on HSLA steel samples are most inconsistent when higher current (33A) was used. Perhaps the high current and temperature accelerate the corrosion process in this ferrous alloy and interfere with the EDM process. Significant corrosion on steel sample was seen if leaving EDM sample in the air-conditioned room for a day.

Material with high melting temperature requires higher EDM spark energy to melt. Low thermal conductivity and thermal diffusivity result in more heat loss when heat is transferred from a spark through the dielectric layer and into the material workpiece.

Figures 12-15, plotting on the log-log scale, illustrate the dependence of MRR on the above-mentioned variables. The average of MRR data are used to fit a line through. The slope of each line, or the exponent of the power equation, indicates the effect of those variables on MRR. The calculated thermal conductivity and diffusivity of pewter, however, do not follow the trend and are excluded from the data fitting calculation. The fitness value R^2 is 84.8% for charge per cycle line (Figure 12), 98.5% for melting temperature line (Figure 13), 89.9% for diffusivity line (Figure 15), but is only 46.6% for conductivity line (Figure 14).

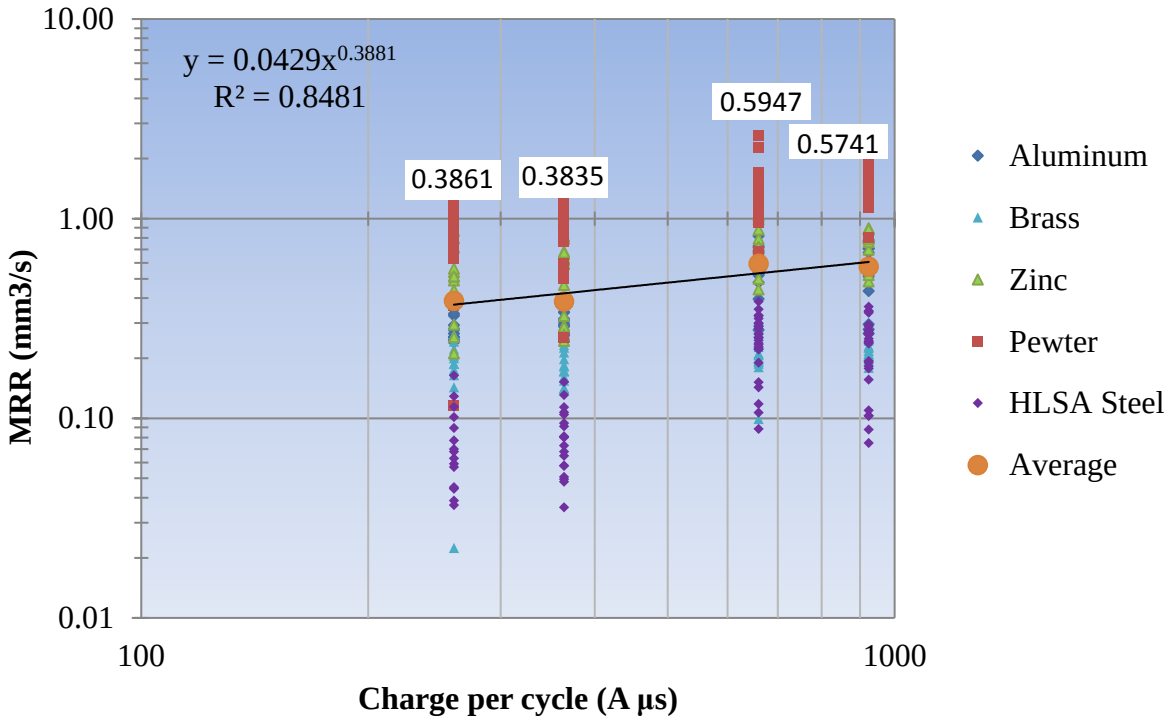

Figure 12: Effect of MRR on charge per cycle

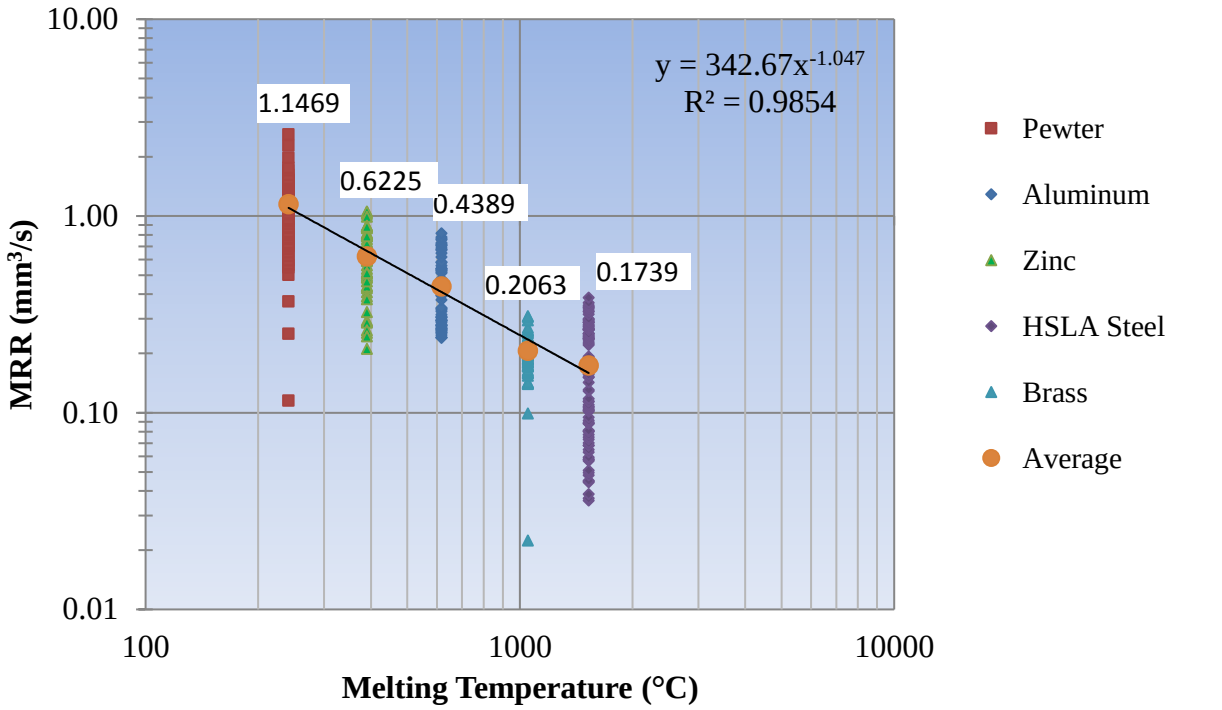

Figure 13: Effect of MRR on workpiece melting temperature

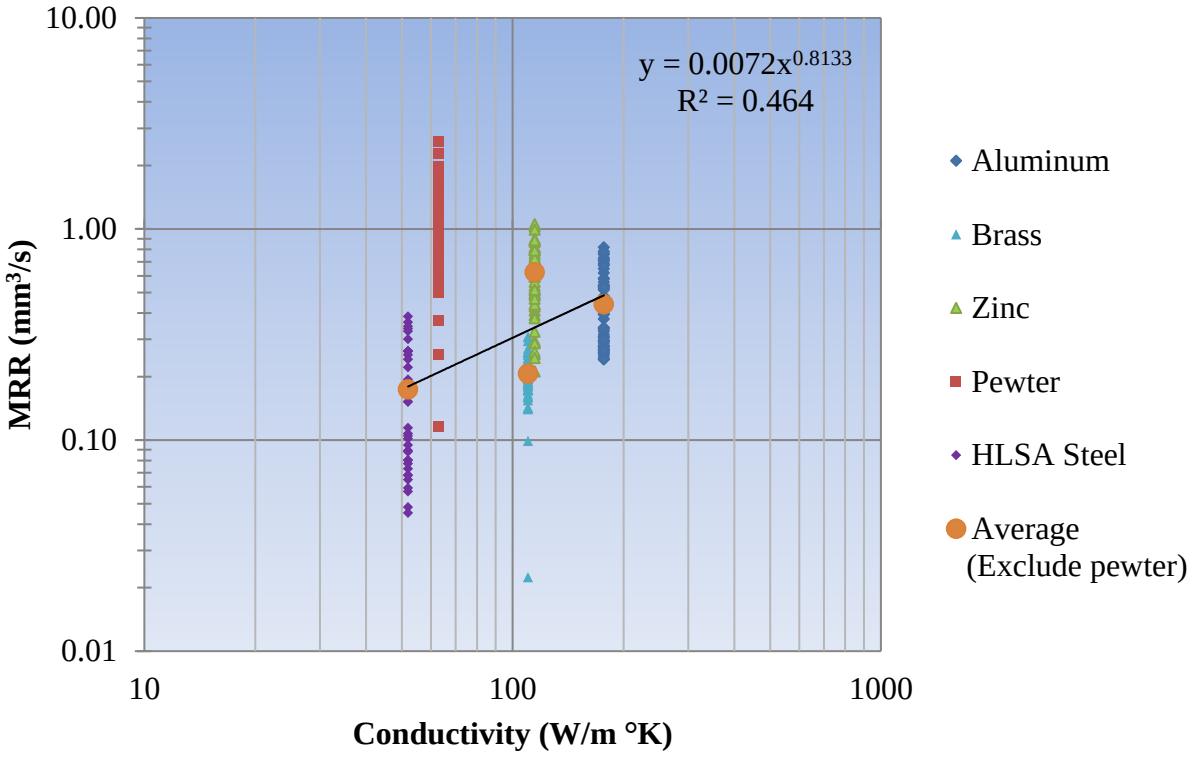

Figure 14: Effect of MRR on workpiece thermal conductivity

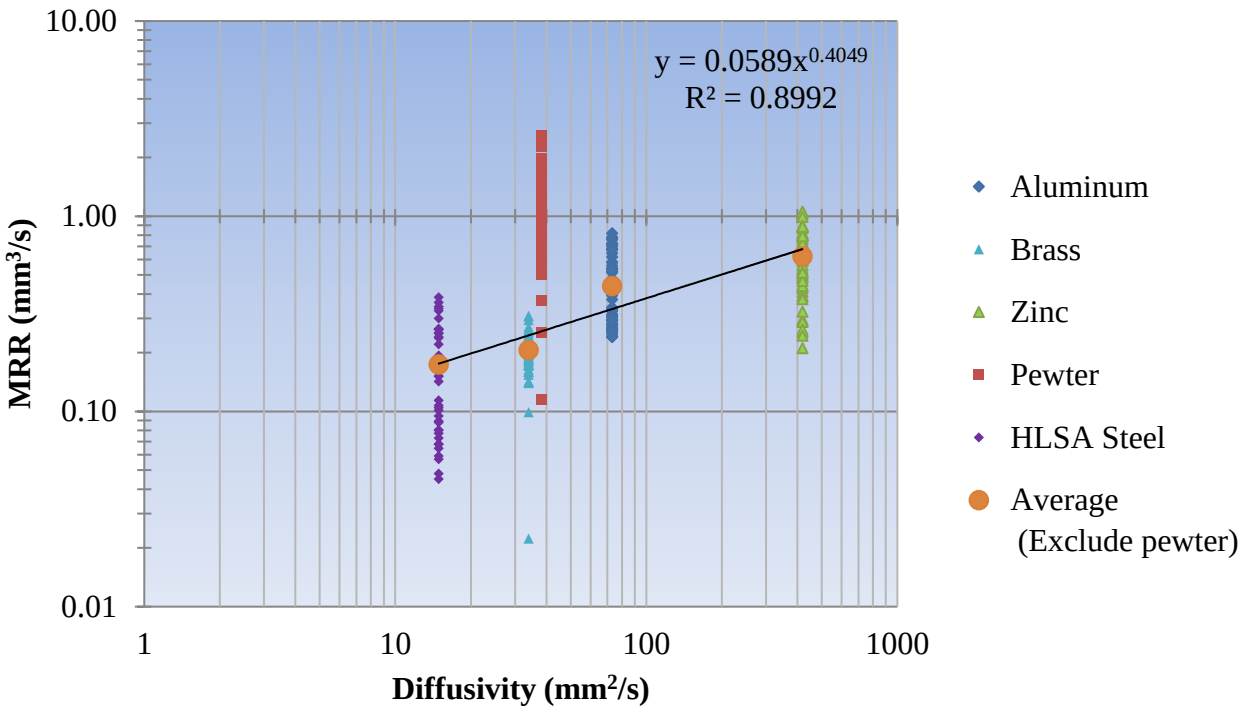

Figure 15: Effect of MRR on workpiece thermal diffusivity

The MRR data suggest the dependence of MRR on both process variables and thermal properties of a workpiece:

$$MRR = P\ {Q_c}^{a}\ K^{b}\ D^{c}\ {T_m}^{d}$$

$$MRR = P\ {Q_c}^{0.3881}\ K^{0.2796}\ D^{0.3903}\ {T_m}^{-1.061} \qquad (6)$$

Where
MRR: material removal rate (mm^3/s)
P: proportional constant
Q_c: charge per cycle (A μs)
D: diffusivity (mm^2/s)
K: conductivity (W/m °K)
T_m: workpiece melting temperature (°C)

The experimental data for MRR are then plotted against calculated values from the Current model (equation 2), the Charge model (equation 3), and the Charge-per-cycle model (equation 6) assuming the proportional constant *P* = 1. The Current model, including current and melting

temperature, has the highest percent error of ~1000% on the average (Figure 16). The Charge model, including charge (product of current and on-time) and melting temperature, produces ~90% error (Figure 17). The Charge-per-cycle model, including the effective charge and other thermal properties, produces ~ 30% error for aluminum (Figure 18a), but ~ 60% error when including all 5 tested materials (Figure 18b).

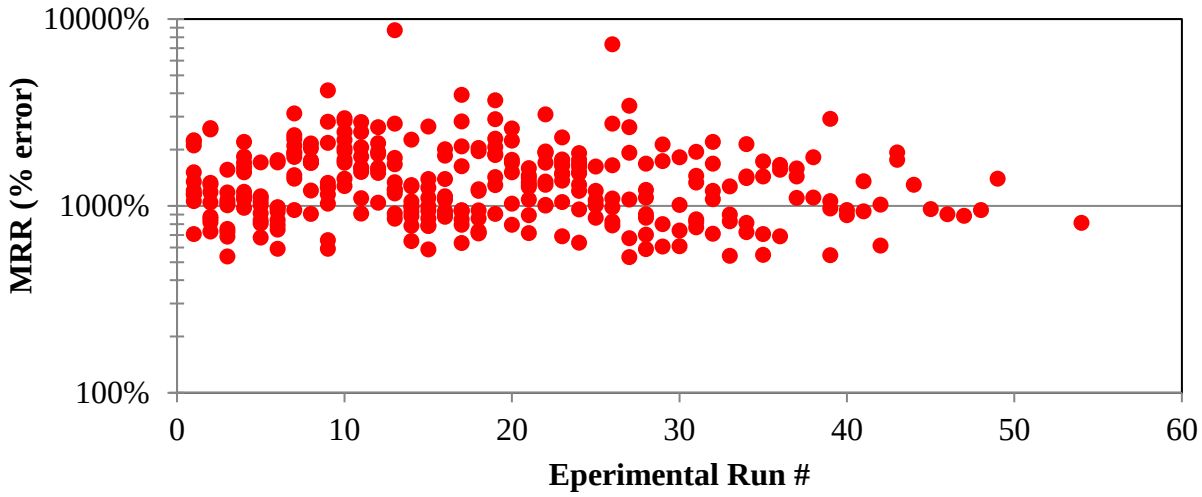

Figure 16: Deviation of calculated MMR (current model, equation 2) and experimental MRR for all materials. The absolute error percentages are used.

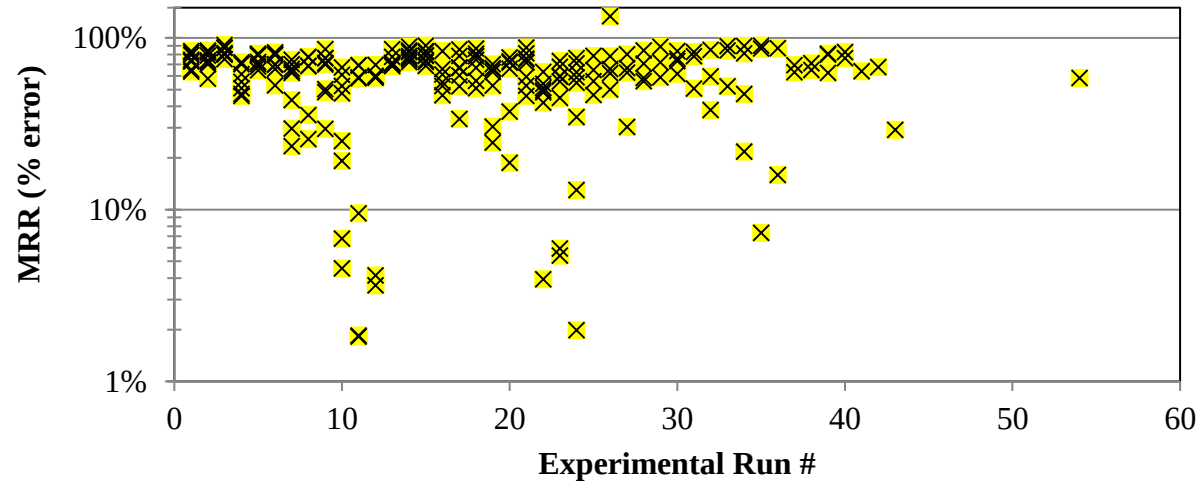

Figure 17: Deviation of calculated MMR (charge model, equation 2) and experimental MRR for all materials. The absolute error percentages are used.

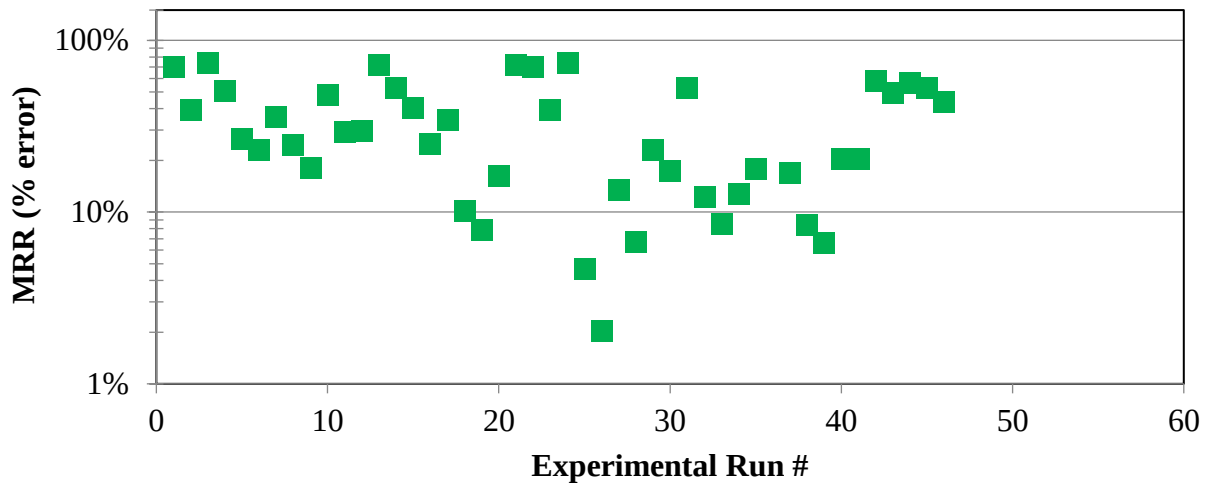

Figure 18a: Deviation of calculated MMR (charge-per-cycle model, equation 6) and experimental MRR for aluminum only. The absolute error percentages are used.

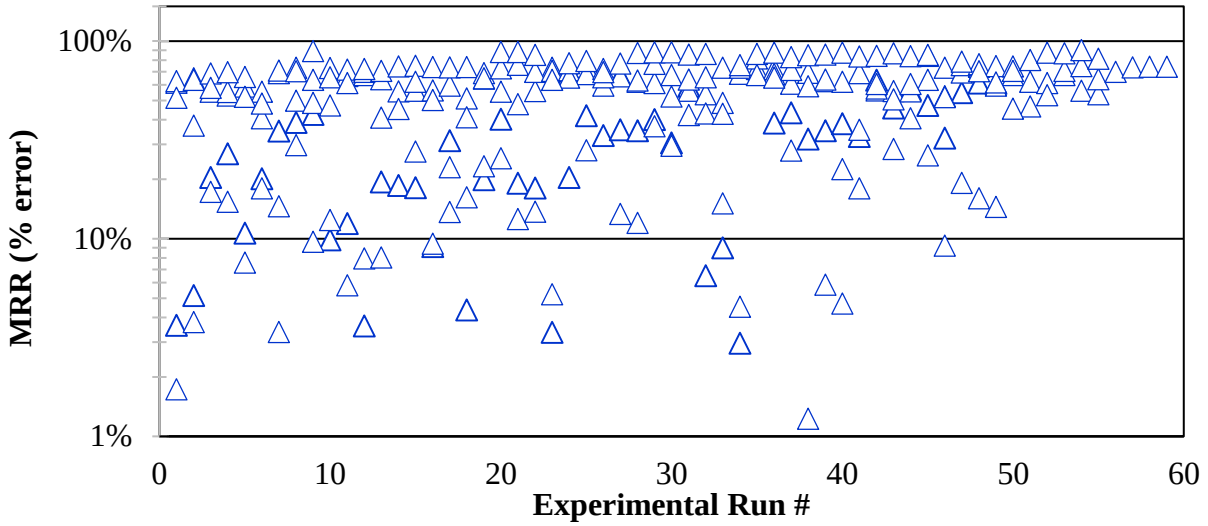

Figure 18b: Deviation of calculated MMR (charge-per-cycle model, equation 6) and experimental MRR for all materials. The absolute error percentages are used.

CHAPTER IV

CONCLUSION

A new empirical model was derived to predict material removal rate (MRR) in die-sinking Electrical Discharge Machining. Comparison of the new model and classical model against experimental data was performed. The study utilized five different engineering materials with spreading melting temperatures. It was shown that:

1) The new model includes charge per cycle (current and on-time) while the classical model uses current only. Both model show strong dependence of MRR on melting temperature. The power exponent was calculated to be -1.061 versus that of -1.23 from the classical model for MRR.
2) The new model includes thermal conductivity and thermal diffusivity of workpiece material.
3) The new model predicts MRR within 32% error for aluminum, and ~ 60% for all five materials. This is a significant achievement since the classical model produces ~1000 % error.

Future Work

Future work can be performed to further enhance the derived model.

a) There is an overlap between thermal conductivity and thermal diffusivity. Perhaps thermal diffusivity would replace thermal conductivity in the revised model. Calculation of thermal diffusivity, however, requires the value of thermal conductivity, which is measurable with a suitable instrument.

b) The new model assumes unity of the proportional constant. Additional work should be done to optimize this constant to further enhance the model accuracy.

c) Corrosion prone material, such as steel, should have the surfaces ground to effectively remove all corrosion products. Hand sanding would not be sufficient and contribute to data variation due to remaining corrosion product on the surface.

REFERENCES

[1] American Society for Metals. http://asm.matweb.com [retrieved 20 May 2016].

[2] AZO Materials. http://www.azom.com/article.aspx?ArticleID=9288 [retrieved 20 January 2017].

[3] Electronics-Cooling.com. http://www.electronics-cooling.com/2007/08/thermal-diffusivity [retrieved 12 February 2017].

[4] Izwan, N. S. L. B., Feng, Z., Patel, J. B., and Hung, W. N. (2016). Prediction of material removal rate in die-sinking electrical discharge machining. Proceedings, NAMRC 44-102, North American Manufacturing Research Conference, Virginia.

[5] MakeItFrom.com. http://www.makeitfrom.com [retrieved 20 May 2016].

[6] Material Properties Data. http://www.matweb.com [retrieved 10 April 2017]

[7] Radio-Electronics.com. http://www.radio-electronics.com/info/formulae/resistance/resistivity-table.php [retrieved 12 February 2017].

[8] RotoMetals.com. https://rotometals.com/alloy-r92-pewter-casting-ingot-92-tin-8-antimony [retrieved 30 January 2017].

[9] Scifinder.org. http://origin-scifinder.cas.org/scifinder/view/scifinder/scifinderExplore.jsf [retrieved 12 February 2017].

[10] Weller E.J., editor. (1984). Nontraditional Machining Processes, 2nd edition. Dearborn, Mich: Society of Manufacturing Engineers. ISBN 9780872631335.

APPENDIX A

EDM SETTINGS PER GROUP

Group Number	On Time (μs)	Off Time (μs)	Current (A)	Capacitance (μF)	Capacitor Switch ON	Servo Voltage Regulator
1	20	20	13	0.22	C5	8 (44 V)
2	20	10	13	0.22	C5	8 (44 V)
3	20	4	13	0.22	C5	8 (44 V)
4	28	28	13	0.22	C5	8 (44 V)
5	28	14	13	0.22	C5	8 (44 V)
6	28	6	13	0.22	C5	8 (44 V)
7	20	20	33	0.22	C5	8 (44 V)
8	20	10	33	0.22	C5	8 (44 V)
9	20	4	33	0.22	C5	8 (44 V)
10	28	28	33	0.22	C5	8 (44 V)
11	28	14	33	0.22	C5	8 (44 V)
12	28	6	33	0.22	C5	8 (44 V)

APPENDIX B

CALCULATE THERMAL CONDUCTIVITY

The proposed equation to calculate thermal conductivity is modeled after the rule of mixture and electrical conductivity of an alloy is repeated from the main text:

$$\frac{100}{K_{alloy}} = \sum_{i=1}^{n} \frac{x_i}{K_i} \tag{4}$$

Where K_{alloy}: thermal conductivity of an alloy (W/m°K)

n: number of elements in alloy

K_i: thermal conductivity to the ith element (W/m°K)

x_i: volume percentage of element i (%)

- Thermal conductivity of ZA-8 zinc aluminum elements (89.8 Zn, 8.8 Al, 1.3 Cu) are: 112.2, 210, and 385 W/m°K for Zn, Al, and Cu respectively (www.matweb.com). Equation (4) becomes:

$$\frac{100}{K_{ZA8}} \approx \frac{89.8}{112.2} + \frac{8.8}{210} + \frac{1.3}{385}; or\ K_{ZA8} = 118\ W/m°K$$

  The calculated value is 2.6% different from the published value of 114.7 W/m°K (Table 2).

- The thermal conductivity of CA360 brass elements (61.5 Cu, 0.35 Fe, 3.0 Pb, 35.5 Zn) are: 38.5, 76.2, 33.0, and 112.2 W/m°K for Cu, Fe, Pb and Zn respectively (www.matweb.com). Equation (4) becomes:

$$\frac{100}{K_{brass}} = \frac{61.5}{385} + \frac{0.35}{76.8} + \frac{3.0}{33.0} + \frac{35.5}{112.2}; or\ K_{brass} = 174.9\ \text{W/m°K}$$

  The calculated value is 63% different from the published value of 110 W/m°K (Table 4).

- The thermal conductivity of Pewter R92 elements (92 Sn, 8 Sb) are: 63 and 18.6 W/m°K for Sn and Sb respectively (www.matweb.com). Equation (4) becomes:

$$\frac{100}{K_{pewter}} = \frac{92}{385} + \frac{8}{18.6}; \; or \; K_{pewter} = 52.9 \; \mathrm{W/m°K}$$

APPENDIX C

RAW DATA FOR ALUMINUM

Current (A)	*On Time (μs)*	*Off Time (μs)*	*Charge (A*μs)*	*Experimental MRR (mm^3/s)*	*Current model MRR (mm^3/s)*	*Charge model MRR (mm^3/s)*	*Charge per cycle model MRR (mm^3/s)*
13	20	20	260	0.1427	3.1920	0.0695	0.2430
13	20	10	260	0.1744	3.1920	0.0695	0.2430
13	28	28	364	0.1399	3.1920	0.0695	0.2430
13	28	6	364	0.1611	3.1920	0.1009	0.2430
33	20	20	660	0.1918	3.1920	0.1009	0.2431
33	20	10	660	0.1976	3.1920	0.1009	0.2431
33	28	28	924	0.1790	8.1027	0.1954	0.2431
33	28	14	924	0.1949	8.1027	0.1954	0.2431
33	28	6	924	0.2059	8.1027	0.1954	0.2431
13	20	20	260	0.1641	8.1027	0.2838	0.2430
13	20	10	260	0.1878	8.1027	0.2838	0.2430
13	20	4	260	0.1871	8.1027	0.2838	0.2430
13	28	28	364	0.1411	3.1920	0.0695	0.2430
13	28	14	364	0.1589	3.1920	0.0695	0.2430
13	28	6	364	0.1731	3.1920	0.0695	0.2430
33	20	20	660	0.1945	3.1920	0.1009	0.2431
33	20	10	660	0.1806	3.1920	0.1009	0.2431
33	20	4	660	0.2707	3.1920	0.1009	0.2431
33	28	14	924	0.2255	8.1027	0.1954	0.2431
33	28	6	924	0.2092	8.1027	0.1954	0.2431
13	28	28	364	0.1415	8.1027	0.1954	0.2430
13	28	28	364	0.1427	8.1027	0.2838	0.2430
13	28	28	364	0.1744	8.1027	0.2838	0.2430
13	28	28	364	0.1399	8.1027	0.2838	0.2430
13	20	20	260	0.2548	3.1920	0.1009	0.2430
13	20	10	260	0.2480	3.1920	0.1009	0.2430
13	20	4	260	0.2805	3.1920	0.1009	0.2430
13	28	28	364	0.2606	3.1920	0.1009	0.2430
13	28	14	364	0.3152	8.1027	0.1954	0.2430
13	28	6	364	0.2947	8.1027	0.1954	0.2430
33	20	20	660	0.5193	8.1027	0.1954	0.2431
33	20	4	660	0.2769	3.1920	0.1954	0.2431
33	28	28	924	0.2659	8.1027	0.2838	0.2431
33	28	14	924	0.2788	8.1027	0.2838	0.2431
33	28	6	924	0.2961	8.1027	0.0695	0.2431
13	20	20	260	0.2408	8.1027	0.1954	0.2430
13	20	10	260	0.2927	8.1027	0.1954	0.2430
13	20	4	260	0.2653	8.1027	0.1954	0.2430
13	28	28	364	0.2602	8.1027	0.2838	0.2430
13	28	14	364	0.3053	8.1027	0.1954	0.2430
13	28	6	364	0.3052	8.1027	0.2838	0.2430
33	20	20	660	0.5825	8.1027	0.0695	0.2431
33	20	4	660	0.4793	8.1027	0.0695	0.2431

Appendix C continued.

Current (A)	*On Time (μs)*	*Off Time (μs)*	*Charge (A*μs)*	*Experimental MRR (mm^3/s)*	*Current model MRR (mm^3/s)*	*Charge model MRR (mm^3/s)*	*Charge per cycle model MRR (mm^3/s)*
33	28	28	924	0.5596	8.1027	0.0695	0.2431
33	28	14	924	0.5137	8.1027	0.1009	0.2431

APPENDIX D: RAW DATA FOR BRASS

Current (A)	*On Time (μs)*	*Off Time (μs)*	*Charge (A*μs)*	*Experimental MRR (mm^3/s)*	*Current model MRR (mm^3/s)*	*Charge model MRR (mm^3/s)*
13	20	20	260	0.1427	1.6598	0.0522
13	20	10	260	0.1744	1.6598	0.0522
13	28	28	364	0.1399	1.6598	0.0522
13	28	6	364	0.1611	1.6598	0.0759
33	20	20	660	0.1918	1.6598	0.0759
33	20	10	660	0.1976	1.6598	0.0759
33	28	28	924	0.1790	4.2133	0.1468
33	28	14	924	0.1949	4.2133	0.1468
33	28	6	924	0.2059	4.2133	0.1468
13	20	20	260	0.1641	4.2133	0.2133
13	20	10	260	0.1878	4.2133	0.2133
13	20	4	260	0.1871	4.2133	0.2133
13	28	28	364	0.1411	1.6598	0.0522
13	28	14	364	0.1589	1.6598	0.0522
13	28	6	364	0.1731	1.6598	0.0522
33	20	20	660	0.1945	1.6598	0.0759
33	20	10	660	0.1806	1.6598	0.0759
33	20	4	660	0.2707	1.6598	0.0759
33	28	28	924		4.2133	0.1468
33	28	14	924	0.2255	4.2133	0.1468
33	28	6	924	0.2092	4.2133	0.1468
13	28	28	364	0.1415	4.2133	0.2133
13	20	20	260	0.2056	4.2133	0.2133
13	20	10	260	0.2000	4.2133	0.2133
13	20	4	260	0.2612	1.6598	0.0759
13	28	28	364	0.1542	1.6598	0.0522
13	28	14	364	0.2137	1.6598	0.0522
13	28	6	364		1.6598	0.0759
33	20	20	660	0.2087	1.6598	0.0759
33	20	10	660	0.2277	1.6598	0.0759
33	28	28	924	0.2041	4.2133	0.1468
33	28	14	924	0.2173	4.2133	0.1468
33	28	6	924	0.2116	4.2133	0.1468
13	20	20	260	0.1738	4.2133	0.2133
13	20	10	260	0.2219	4.2133	0.2133
13	20	4	260	0.2423	1.6598	0.0522
13	28	28	364	0.1596	1.6598	0.0759
13	28	14	364	0.2262	4.2133	0.1468
13	28	6	364		1.6598	0.0759
33	20	20	660	0.2110	1.6598	0.0522
33	20	10	660	0.2337	1.6598	0.0522
33	28	28	924	0.2053	1.6598	0.0522
33	28	14	924	0.2268	1.6598	0.0759
33	28	6	924	0.2452	1.6598	0.0759
13	28	28	364	0.1719	1.6598	0.0759
13	20	20	260	0.2056	4.2133	0.1468
13	20	10	260	0.2000	4.2133	0.1468

Appendix D Continued.

Current (A)	*On Time (µs)*	*Off Time (µs)*	*Charge (A*µs)*	*Experimental MRR (mm^3/s)*	*Current model MRR (mm^3/s)*	*Charge model MRR (mm^3/s)*
13	20	4	260	0.2612	4.2133	0.1468
13	28	28	364	0.1542	4.2133	0.2133
13	28	14	364	0.2137	4.2133	0.2133
13	28	6	364		4.2133	0.2133
33	20	20	660	0.2087	1.6598	0.0522
33	20	10	660	0.2277	1.6598	0.0522
33	20	4	660	0.2946	1.6598	0.0522
33	28	28	924	0.2041	1.6598	0.0759
33	28	14	924	0.2173	1.6598	0.0759
33	28	6	924	0.2116	1.6598	0.0759
13	20	20	260	0.1738	4.2133	0.1468
13	20	10	260	0.2219	4.2133	0.1468
13	20	4	260	0.2423	4.2133	0.1468
13	28	28	364	0.1596	4.2133	0.2133
13	28	14	364	0.2262	4.2133	0.2133
33	20	20	660	0.2110	4.2133	0.2133
33	20	10	660	0.2337	1.6598	0.0759
33	20	4	660	0.3092	1.6598	0.0522
33	28	28	924	0.2053	1.6598	0.0522
33	28	14	924	0.2268	1.6598	0.0759
33	28	6	924	0.2452	1.6598	0.0759
13	20	20	260	0.1719	1.6598	0.0759
13	20	4	260	0.2630	4.2133	0.1468
13	28	28	364	0.1719	4.2133	0.1468
13	28	14	364	0.1845	4.2133	0.1468
13	28	6	364	0.1978	4.2133	0.2133
33	20	10	660	0.2367	4.2133	0.2133
33	20	4	660	0.3066	1.6598	0.0522
33	28	28	924	0.1877	1.6598	0.0759
33	28	14	924	0.2302	4.2133	0.1468
33	28	6	924	0.2536	1.6598	0.0759
13	20	4	260	0.2574	1.6598	0.0522
13	28	6	364	0.2326	1.6598	0.0522
33	20	20	660	0.2069	1.6598	0.0522
13	28	6	364	0.1818	1.6598	0.0759

APPENDIX E: RAW DATA FOR PEWTER

Current (A)	*On Time (μs)*	*Off Time (μs)*	*Charge (A*μs)*	*Experimental MRR (mm^3/s)*	*Current model MRR (mm^3/s)*	*Charge model MRR (mm^3/s)*
13	20	20	260	0.6282	10.1445	0.1151
13	20	10	260	0.7230	10.1445	0.1151
13	20	4	260	0.9142	10.1445	0.1151
13	28	28	364	0.5954	10.1445	0.1672
13	28	6	364	0.5459	10.1445	0.1672
33	20	20	660	1.0803	10.1445	0.1672
33	20	10	660	1.4132	25.7514	0.3237
33	20	4	660	1.1326	25.7514	0.3237
33	28	28	924	1.4277	25.7514	0.3237
33	28	14	924	1.5248	25.7514	0.4702
33	28	6	924	1.5482	25.7514	0.4702
13	20	20	260	0.8005	25.7514	0.4702
13	20	10	260	1.0333	10.1445	0.1151
13	20	4	260	1.1537	10.1445	0.1151
13	28	28	364	1.0213	10.1445	0.1151
13	28	14	364	1.1367	10.1445	0.1672
13	28	6	364	1.2419	10.1445	0.1672
33	20	20	660	1.0792	10.1445	0.1672
33	20	10	660	1.3833	25.7514	0.3237
33	20	4	660	1.7081	25.7514	0.3237
33	28	28	924	1.2751	25.7514	0.3237
33	28	14	924	1.4626	25.7514	0.4702
33	28	6	924	1.6169	25.7514	0.4702
13	28	28	364	0.8391	25.7514	0.4702
13	28	6	364	1.1703	25.7514	0.3237
13	20	20	260	0.6992	25.7514	0.3237
13	20	10	260	0.7112	10.1445	0.1672
13	20	4	260	1.2285	10.1445	0.1672
13	28	28	364	0.5620	25.7514	0.3237
13	28	14	364	0.8276	25.7514	0.3237
13	28	6	364	0.9406	10.1445	0.1151
33	20	20	660	1.2686	10.1445	0.1151
33	20	10	660	1.4208	10.1445	0.1151
33	28	28	924	1.2050	10.1445	0.1151
33	28	14	924	1.5114	10.1445	0.1672
33	28	6	924	1.1364	10.1445	0.1672
13	20	20	260	0.1152	25.7514	0.4702
13	20	10	260	0.7284	25.7514	0.4702
13	20	4	260	0.3675	10.1445	0.1672
13	28	14	364	0.2521	10.1445	0.1672
13	28	6	364	0.7645	10.1445	0.1151
33	20	20	660	0.6815	10.1445	0.1151
33	20	10	660	0.9556	10.1445	0.1151
33	20	4	660		10.1445	0.1672
33	28	28	924	0.8083	10.1445	0.1672
33	28	14	924	1.7559	10.1445	0.1672
33	28	6	924	1.9767	25.7514	0.3237

Appendix E Continued.

Current (A)	*On Time (µs)*	*Off Time (µs)*	*Charge (A*µs)*	*Experimental MRR (mm^3/s)*	*Current model MRR (mm^3/s)*	*Charge model MRR (mm^3/s)*
33	20	10	660	1.4908	25.7514	0.3237
33	20	10	660	1.4705	25.7514	0.3237
13	28	28	364	0.5009	25.7514	0.4702
33	20	20	660	1.1532	25.7514	0.4702
33	20	20	660	1.3397	25.7514	0.4702
13	20	20	260	0.6553	10.1445	0.1151
13	20	20	260	0.7777	10.1445	0.1151
13	20	4	260	1.0917	10.1445	0.1151
13	20	4	260	1.1115	10.1445	0.1672
13	28	6	364	1.2564	10.1445	0.1672
13	28	6	364	1.2881	10.1445	0.1672
33	28	28	924	1.5265	25.7514	0.3237
33	28	28	924	1.3421	25.7514	0.3237
13	28	14	364	0.8740	25.7514	0.3237
13	28	14	364	0.9658	25.7514	0.4702

APPENDIX F: RAW DATA FOR STEEL

Current (A)	*On Time (μs)*	*Off Time (μs)*	*Charge (A*μs)*	*Experimental MRR (mm^3/s)*	*Current model MRR (mm^3/s)*	*Charge model MRR (mm^3/s)*
13	20	20	260	0.0447	1.0471	0.0427
13	20	10	260	0.0386	1.0471	0.0427
13	20	4	260	0.0630	1.0471	0.0427
13	28	28	364	0.0813	1.0471	0.0620
13	28	14	364	0.0578	1.0471	0.0620
13	28	6	364	0.0579	1.0471	0.0620
33	20	20	660	0.1068	2.6580	0.1201
33	20	10	660	0.1179	2.6580	0.1201
33	20	4	660	0.3516	2.6580	0.1201
33	28	28	924	0.1028	2.6580	0.1745
33	28	14	924	0.1028	2.6580	0.1745
33	28	6	924	0.1562	2.6580	0.1745
13	20	20	260	0.0367	1.0471	0.0427
13	20	10	260	0.0443	1.0471	0.0427
13	20	4	260	0.0701	1.0471	0.0427
13	28	28	364	0.0496	1.0471	0.0620
13	28	14	364	0.0357	1.0471	0.0620
13	28	6	364	0.0508	1.0471	0.0620
33	20	20	660	0.0883	2.6580	0.1201
33	20	10	660	0.2977	2.6580	0.1201
33	20	4	660	0.3260	2.6580	0.1201
33	28	28	924	0.2392	2.6580	0.1745
33	28	14	924	0.1094	2.6580	0.1745
33	28	6	924	0.1899	2.6580	0.1745
13	20	4	260	0.1287	1.0471	0.0620
13	28	14	364	0.0911	2.6580	0.1201
13	28	6	364	0.1309	2.6580	0.1745
33	20	20	660	0.2458	1.0471	0.0620
33	20	4	660	0.3163	1.0471	0.0427
33	28	28	924	0.2441	1.0471	0.0620
33	28	14	924	0.2891	1.0471	0.0620
33	28	6	924	0.0752	2.6580	0.1201
13	28	14	364	0.1137	1.0471	0.0427
33	20	20	660	0.2284	1.0471	0.0620
33	20	10	660	0.2805	1.0471	0.0427
33	20	4	660	0.2243	2.6580	0.1201
33	28	28	924	0.2371	2.6580	0.1201
33	28	14	924	0.2765	2.6580	0.1201
33	28	6	924	0.3431	2.6580	0.1745
33	20	4	660	0.2343	2.6580	0.1745
33	28	6	924	0.2745	2.6580	0.1745
33	20	4	660	0.2884	2.6580	0.1201
33	28	6	924	0.2673	2.6580	0.1201
33	28	6	924	0.2942	2.6580	0.1201
13	20	20	260	0.0451	2.6580	0.1745
13	20	10	260	0.1143	2.6580	0.1745
13	20	4	260	0.0893	2.6580	0.1745

Appendix F Continued.

Current (A)	*On Time (µs)*	*Off Time (µs)*	*Charge (A*µs)*	*Experimental MRR (mm^3/s)*	*Current model MRR (mm^3/s)*	*Charge model MRR (mm^3/s)*
13	28	28	364	0.0648	2.6580	0.1201
13	28	14	364	0.0946	2.6580	0.1745
13	28	6	364	0.1520	2.6580	0.0427
33	20	20	660	0.2528	2.6580	0.0427
33	20	10	660	0.2644	2.6580	0.0427
33	20	4	660	0.3848	2.6580	0.0620
33	28	28	924	0.1933	2.6580	0.0620
33	28	14	924	0.2631	1.0471	0.0620
13	20	20	260	0.0592	1.0471	0.1201
13	20	10	260	0.1015	1.0471	0.1201
13	20	4	260	0.0774	1.0471	0.1201
13	28	28	364	0.1072	1.0471	0.1745
13	28	14	364	0.0481	1.0471	0.1745
13	28	6	364	0.0804	2.6580	0.1745
33	20	20	660	0.2644	2.6580	0.0427
33	28	28	924	0.2409	2.6580	0.0427
33	28	14	924	0.3373	2.6580	0.0427
33	28	6	924	0.3617	2.6580	0.0620
13	28	28	364	0.0804	2.6580	0.0620
33	20	10	660	0.3001	1.0471	0.0620
33	28	6	924	0.3449	1.0471	0.1201
13	28	6	364	0.1046	1.0471	0.1201
13	20	10	260	0.0570	1.0471	0.1201
13	28	14	364	0.0730	1.0471	0.1745
33	20	4	660	0.3282	1.0471	0.1745
13	20	10	260	0.1636	2.6580	0.1745
13	28	6	364	0.0681	2.6580	0.0620
33	20	20	660	0.1513	2.6580	0.1201
33	20	10	660	0.2208	2.6580	0.1745
33	28	28	924	0.0878	2.6580	0.0620
33	28	6	924	0.1826	2.6580	0.0427
33	20	20	660	0.2380	1.0471	0.0620
33	20	10	660	0.1427	2.6580	0.0620
33	20	4	660	0.1901	2.6580	0.1201
33	28	28	924	0.2507	1.0471	0.0427
33	28	14	924	0.2651	1.0471	0.0620
33	28	6	924	0.2698	1.0471	0.0427
33	20	4	660	0.2532	1.0471	0.1201
33	28	14	924	0.1775	2.6580	0.1201

APPENDIX G: RAW DATA FOR ZINC

Current (A)	*On Time (μs)*	*Off Time (μs)*	*Charge (A*μs)*	*Experimental MRR (mm^3/s)*	*Current model MRR (mm^3/s)*	*Charge model MRR (mm^3/s)*
13	20	20	260	0.4294	5.6207	0.0889
13	20	10	260	0.4904	5.6207	0.0889
13	20	4	260	0.4385	5.6207	0.0889
13	28	28	364	0.2443	5.6207	0.1292
13	28	14	364	0.4657	5.6207	0.1292
13	28	6	364	0.6315	5.6207	0.1292
33	20	20	660	0.7388	14.2678	0.2501
33	20	10	660	0.7933	14.2678	0.2501
33	20	4	660	1.0519	14.2678	0.2501
33	28	28	924	0.7639	14.2678	0.3634
33	28	14	924	0.8818	14.2678	0.3634
33	28	6	924	0.8894	14.2678	0.3634
13	20	20	260	0.3908	5.6207	0.0889
13	20	10	260	0.5131	5.6207	0.0889
13	20	4	260	0.5134	5.6207	0.0889
13	28	28	364	0.3766	5.6207	0.1292
13	28	14	364	0.5936	5.6207	0.1292
13	28	6	364	0.6762	5.6207	0.1292
33	20	20	660	0.7230	14.2678	0.2501
33	20	10	660	0.8829	14.2678	0.2501
33	20	4	660	0.9923	14.2678	0.2501
33	28	28	924	0.7898	14.2678	0.3634
33	28	14	924	0.8944	14.2678	0.3634
33	28	6	924	0.8840	14.2678	0.3634
13	20	20	260	0.2548	5.6207	0.1292
13	20	10	260	0.2111	14.2678	0.2501
13	20	4	260	0.7158	14.2678	0.3634
13	28	28	364	0.2899	5.6207	0.1292
13	28	14	364	0.6207	5.6207	0.0889
13	28	6	364	0.6635	5.6207	0.1292
33	20	20	660	0.4416	5.6207	0.1292
33	20	4	660	1.0494	14.2678	0.2501
33	28	28	924	0.4850	5.6207	0.0889
13	20	20	260	0.2949	5.6207	0.1292
13	20	4	260	0.5389	5.6207	0.0889
13	28	28	364	0.2872	5.6207	0.0889
13	28	14	364	0.3250	5.6207	0.0889
13	28	6	364	0.2623	5.6207	0.0889
33	20	4	660	1.0257	5.6207	0.1292
33	28	28	924	0.6988	5.6207	0.1292
33	28	14	924	0.8197	5.6207	0.1292
33	28	6	924	0.8001	14.2678	0.2501
33	20	10	660	0.4991	14.2678	0.2501
33	28	6	924	0.5212	14.2678	0.2501
13	28	6	364	0.8166	14.2678	0.3634
13	20	10	260	0.7969	14.2678	0.3634
13	28	6	364	0.7931	14.2678	0.3634

Appendix G Continued.

Current (A)	*On Time (µs)*	*Off Time (µs)*	*Charge (A*µs)*	*Experimental MRR (mm^3/s)*	*Current model MRR (mm^3/s)*	*Charge model MRR (mm^3/s)*
13	28	14	364	0.5924	5.6207	0.0889
33	20	4	660	0.6196	5.6207	0.0889
13	20	10	260	0.5619	5.6207	0.0889
13	28	6	364	0.6825	5.6207	0.1292
13	20	10	260	0.8676	5.6207	0.1292